13

Layer-by-layer chemical and phase analysis of ultrathin niobium nitride films

© O.I. Lubenchenko, A.V. Lubenchenko, D.S. Lukyantsev, D.A. Ivanov, I.V. Ivanova, O.N. Pavlov

National Research University Moscow Power Engineering Institute
111250 Moscow, Russia
e-mail: IvanovaOII@mpei.ru

Received April 25, 2025
Revised April 25, 2025
Accepted April 25, 2025

The study investigated various ultrathin niobium nitride films that differed in the type of substrate, presence of a buffer layer, surface oxidation time and rate, and ion beam impact. Depth profiling of ultrathin niobium nitride films was carried out by a non-destructive method for chemical and phase depth profiling using (or based on) X-ray photoelectron spectroscopy. The study has shown that a layer with a modified niobium nitride phase was formed under the oxide layer during atmospheric oxidation of ultrathin niobium nitride film; a 1 nm interface layer was formed when niobium nitride ultrathin film was deposited on an oxidized silicon substrate by magnetron sputtering; no interface layer was formed when ultrathin niobium nitride film was deposited onto a sapphire substrate; oxide layer thickness and phase composition depended on the niobium nitride film oxidation time and rate; not only the NbN film thickness, but also the phase composition of changed under the action of ion beam evaporation.

Keywords: niobium nitride, ultrathin films, X-ray photoelectron spectroscopy, chemical phase depth profiling.

DOI: 10.61011/TP.2025.10.62082.66-25

Introduction

Since the first studies focused on a HEB mixer (a hot electron bolometer mixer or a mixer based on the effect of electronic heating in superconducting films) [1,2] and SSPD (superconducting single-photon detectors) [3], ultrathin metal-nitride films have been playing a key role in creating nanoelectronic devices. Functional properties of nanoelectronic devices depend on thin film structure and chemical and phase depth profile. Owing to its superconducting properties, niobium and niobium compounds (NbN, NbTiN) have become the main materials for films used in nanoelectronics (see, for example, [4] for HEB and [5] for SSPD). Employment of ultrathin VN film for SSPD was reported in [6]. Evolution of normal and superconducting properties of epitaxial TiN thin films with typical high Ioffe-Regel parameters depending on the film thickness was reported in [7].

To improve functional properties of nanoelectronic devices (increasing intermediate frequency band, decreasing noise temperature), a buffer layer is introduced between the ultrathin film and substrate: MgO [8], AlN [9], 3C-SiC [10], GaN and AlGaN [11]. These studies investigated film structures using HRTEM (high resolution transmission electron microscopy). For HRTEM examination, a special adhesive or titanium layer was applied on top of samples. This allowed investigating the film and buffer layer interface, but distorted the structure of the upper film boundary. Dependence of the superconducting junction temperature on the type of buffer layer is described in [11]. NbN films on a GaN buffer layer turned out to have the highest superconducting junction temperature ($T_c = 13.2\,\mathrm{K}$).

Nb is prone to heavy oxidation and, because most niobium oxides have dielectric properties, their appearance on the surface of superconducting devices adversely affects the functionality of such devices. A large volume of studies, for example, [12] focuses on investigating niobium oxide and niobium nitride films. Formation of an interface between niobium nitride and niobium oxide layers may induce various phases of both niobium oxide and niobium nitride [13]. Study [14] investigated Nb and NbN thin films after thermal and plasma oxidation. Temperature turned out to have a greater effect on the oxidation of Nb than of NbN. Study [15] investigated the oxygen ion irradiation effect on the transformation of superconducting NbN thin films into niobium oxide. The authors showed that such transformation was followed by a corresponding increase in film thickness without signs of evaporation and, thus, enables formation of dielectric regions with desired dimensions and shape during fabrication of various functional components; dependence of NbN thin film resistance on oxygen ion irradiation doses was shown. Study [16] investigated the relation between the critical temperature and crystal structure of NbN_x phases. The authors confirmed the existence of γ-Nb_4N_3, δ-NbN, ξ-NbN, Nb_4N_5 superlattice in various films made from NbNx. The highest critical temperature was observed in the δ-NbN cubic phase. Study [17] investigated epitaxially grown NbN films on a GaN buffer layer without surface heating and on a Si substrate using a MOCVD method (metalorganic chemical vapour deposition — a chemical vapour deposition method using thermal decomposition (pyrolysis) of metalorganic compounds) without heating and with heating to

650 °C. XPS, electron energy loss spectroscopy in reflection geometry (REELS), high-resolution transmission electron microscopy (HTEM) methods were used to investigate film composition and structure. When films are deposited onto substrates, a transition layer is formed and seriously affects NbN-based HEB properties. For example, phonon relaxation times and free path lengths depend on the interface structure [18]. Study [19] investigated optical and transport properties of a series of sapphire-grown ultrathin NbN films with various thicknesses. Dependences of the superconducting junction temperature T_c, residual electrical resistance on the total film thickness (NbN and Nb_2O_5) were obtained. Layer thicknesses were evaluated using a spectroscopic ellipsometry method.

When a film is deposited onto a substrate, the former is always subjected to stresses due to a mismatch between the substrate and film crystal structures and to the difference of thermal expansion coefficients. Film relaxation and rearrangement lead to restructuring of the film itself and „film-substrate“ interface, formation of various phases with variable composition and interfaces between them. In addition, oxide films and underlying transition layers are formed on the surface during atmospheric oxidation of films. Thus, even inherently homogeneous films have a complex multilayer structure. Understanding of chemical and phase profile of films and film-substrate interface will allow predicting their functional properties and improving the ultrathin film deposition and modification technique.

1. Experimental

Chemical phase depth profiling of ultrathin niobium nitride films was quantitativeperformed by an *in situ* nondestructive quantitative layer-by-layer chemical phase analysis of ultrathin films with a subnanometer accuracy to tens of nanometers on the basis of X-ray photoelectron spectroscopy [20].

X-ray photoelectron spectra were measured using an electron-ion spectroscopy module based on the Nanofab 25 (NT-MDT) platform. Ultra-high oil-free vacuum approximately equal to 10^{-6} Pa was achieved in the analytical chamber. The spectra were recorded by the SPECS Phoibos 225 electrostatic hemispherical energy analyzer using an X-ray gun with a Mg anode. The energy analyzer was calibrated using Cu, Ag and Au samples. Spectrometer energy resolution at Ag $3d_{5/2}$ was 0.78 eV (FWHM) for MgK_α non-monochromatic X-ray radiation. The energy analyzer was set to the FAT mode (Fixed Analyzer Transmission). An energy analyzer lens deceleration energy was set to $E_{pass} = 80$ eV for survey spectra, and to $E_{pass} = 20$ eV for detailed spectra. To neutralize the charging effect and determine spectral line positions, the study uses calibration with O 1*s* referencing.

Niobium nitride films were produced using an Orion magnetron sputtering system made by AJA International Inc. A metallic niobium target (99.9%) was sputtered in argon and nitrogen atmosphere (N_2) [13,21]. Niobium nitride was sputtered on the SiO_2/Si and Al_2O_3 substrates (Sp — sapphire).

After removal from the sputtering chamber and before placement into the analytical chamber, the films were subjected to atmospheric oxidation during a period from several days to several weeks. For some samples, oxidation time was less than 24 hours.

2. Chemical phase depth profiling of oxidized ultrathin niobium nitride films

2.1. Air-oxidized ultrathin niobium films on silicon and sapphire substrates

As the flims were exposed to X-ray radiation, the targets were charged to a potential about few volts. This caused spectral shift towards higher kinetic energies. Since the study addressed films on different substrates (SiO_2/Si and Sp), potential, to which the target was charged, was different: for a film on the SiO_2/Si substrate — 0.7 V, for a film on the sapphire substrate — 3.4 V. This shift was compensated by the oxide peak correction method.

Elemental analysis of ultrathin niobium nitride films identified the following elements: on the oxidized silicon substrate — Nb, C, O, N, Si; on the sapphire substrate — Nb, C, O, N, Al. Figure 1 shows survey X-ray photoelectron spectra of these films: red solid line — film on the SiO_2/Si substrate, blue solid line — film on the Sp substrate.

Phase profiling of ultrathin NbN films on the SiO_2/Si and Sp substrates was performed simultaneously on the N 1*s*, O 1*s*, Nb 3*d* spectral photoelectron lines; for a target on the sapphire substrate — on the Al 2*p* spectral line, and for a target on the oxidized silicon substrate — on the Si 2*p* spectral line. When a sample contains complex (two-/three-component) compounds, they shall be detected on all spectral photoelectron lines of the elements included in these compounds.

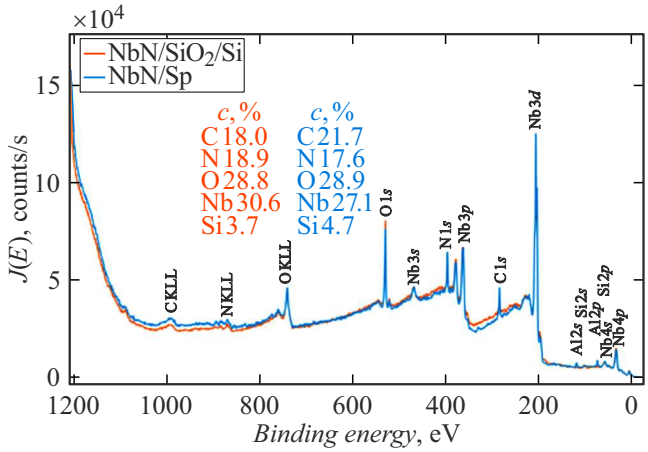

Figure 1. Survey X-ray photoelectron spectra of ultrathin films NbN/SiO_2/Si and NbN/Sp.

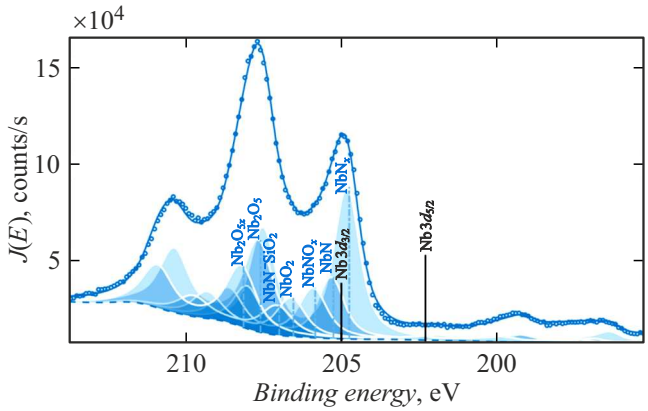

Figure 2. X-ray photoelectron spectrum of the Nb 3*d* line of the ultrathin NbN/SiO_2/Si film.

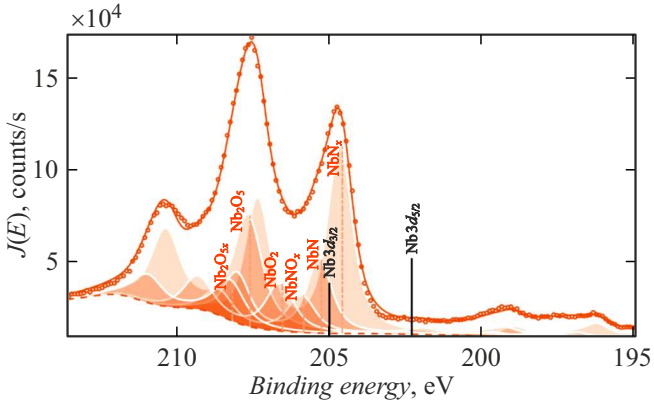

Figure 3. X-ray photoelectron spectrum of the Nb 3*d* line of the ultrathin NbN/Sp film.

Table 1. Phase depth profiling of the ultrathin NbN/SiO_2/Si film

Chemical formula	Binding energy, eV				
	Nb 3*d*	N 1*s*	O 1*s*	Si 2*p*	C 1*s*
NbN	205.3	397.2	–	–	–
NbN_x	204.8	398.3	–	–	–
$NbNO_x$	205.8	399.9	531.2	–	–
NbN-SiO_2	207.1	402.2	532.1	102.9	–
NbO_2	206.5	–	530.6	–	–
Nb_2O_5	207.6	–	530.6	–	–
Nb_2O_{5x}	208.1	–	530.6	–	–
Si	–	–	–	100.2	–
SiO_2	–	–	532.8	103.8	–
CO_x	–	–	533.8	–	286.5
CH_x	–	–	–	–	285.5

Table 2. Phase depth profilng of the ultrathin NbN/Sp film

Chemical formula	Binding energy, eV				
	Nb 3*d*	N 1*s*	O 1*s*	Si 2*p*	C 1*s*
NbN	205.3	397.1	–	–	–
NbN_x	204.6	398.2	–	–	–
$NbNO_x$	205.8	400.1	532.6	–	–
NbO_2	206.5	–	530.8	–	–
Nb_2O_5	207.6	–	530.8	–	–
Nb_2O_{5x}	208.2	–	530.8	–	–
Al_2O_3	–	–	531.6	75.3	–
CO_x	–	–	533.9	–	286.1
CH_x	–	–	–	–	285.4

The study investigated an ultrathin niobium nitride film on an oxidized silicon substrate that had been oxidized in air during several days before placement into the analytical chamber. Analysis of photoelectron lines detected the following: N 1*s* and Nb 3*d* lines — various NbN and NbN_x phases; O 1*s* and Nb 3*d* lines — NbO_2, Nb_2O_5, Nb_2O_{5x} (another phase of the highest niobium oxide with a restructured lattice); N 1*s*, O 1*s* and Nb 3*d* lines — $NbNO_x$; Si 2*p*line — pure silicon; O 1*s* and Si 2*p* lines — SiO_2; N 1*s*, O 1*s*, Nb 3*d* and Si 2*p* lines — NbN-SiO_2 interface phase. Analysis of the C 1*s* line didn't detect free carbon and carbon-niobium compounds, but detected hydrocarbons and CO_x.

Figure 2 shows X-ray photoelectron spectra of the Nb 3*d* lines of the ultrathin NbN film on the SiO_2/Si substrate, respectively. Solid line shows the calculated spectra, circles show the experimental data, dashed line shows the background calculated using method [20,22], partial peaks are filled: The detected phases and their binding energies are shown in Table 1.

The second examined film was the ultrathin niobium nitride film on the sapphire substrate. It was also oxidized in air for several days before placement into the analytical chamber. Analysis of photoelectron lines detected the following: N 1*s* and Nb 3*d* lines - various NbN and NbN_x phases; O 1*s* and Nb 3*d* lines — NbO_2, Nb_2O_5; N 1*s*, O 1*s* and Nb 3*d* lines — $NbNO_x$; O 1*s*, Al 2*s* and Al 2*p* lines — Al_2O_3. Interface phase between the Al_2O_3 and NbN layers wasn't found. Analysis of the C 1*s* line detected hydrocarbons and CO_x. Figure 3 shows X-ray photoelectron spectra of the Nb 3*d* lines of the ultrathin NbN film on the Sp substrate. Solid line shows the calculated spectra, circles show the experimental data, dashed line shows the background calculated using method [22], partial peaks are filled: The detected phases and their binding energies are shown in Table 2.

For depth profiling, a target model is introduced. It is known from the film fabrication history that niobium was deposited in nitrogen and argon atmosphere onto both (oxidized silicon and sapphire) substrates. Then, atmospheric oxidation occurred, and the higher oxide, Nb_2O_5, film was formed on top. The phase analysis detected niobium suboxide and $NbNO_x$ phases. These phases will be assigned to the same layer between the top oxides layer and niobium nitride. The identified various niobium nitride phases are located in different layers. Phase analysis of the ultrathin $NbN/SiO_2/Si$ film identified a phase related to the $NbN\text{-}SiO_2$ interface layer between the substrate and niobium nitride film.

Layer thicknesses were calculated using an equation from [20]:

$$d_i = L_{\text{th}i} \cos\theta \ln\left[\frac{I_i/(n_i\omega_{\gamma\to ei}L_{\text{qa}i})}{\sum\limits_{j=0}^{i-1} I_j/(n_j\omega_{\gamma\to ej}L_{\text{qa}j})} + 1\right]. \quad (1)$$

Here, i is the layer number starting from the surface; d is the layer thickness. L_{th} is the effective attenuation length in a thin layer; θ is the photoelectron escape angle to normal to the surface; I is the photoelectron peak intensity; n is the atom concentration; $\omega_{\gamma\to e}$ is the differential photoelectron production cross-section; L_{qa} is the effective attenuation length in a semi-infinite medium.

Layer thickness calculation error Δd_i is determined using a standard indirect measurement error procedure. According to equation (1), the following equation was derived for the i-th layer thickness error:

$$\Delta d_i = d_i \delta\lambda \sqrt{k_{1i}^2 + k_{2i}^2}, \quad (2)$$

where $\delta\lambda$ is the relative error of inelastic mean free path,

$$k_{1i} = \frac{0.8L_{\text{th}}i}{1 - 0.8L_{\text{th}}i},$$

$$k_{2i} = \sqrt{2\frac{\delta\lambda^2 + \delta n^2 + \delta I^2 + \delta\omega^2}{\delta\lambda} \cdot \frac{B_i}{(B_i+1)\ln(B_i+1)}},$$

$$B_i = \frac{I_i/(n_i\omega_{\gamma\to ei}L_{\text{qa}i})}{\sum\limits_{j=0}^{i-1} I_j/(n_j\omega_{\gamma\to ej}L_{\text{qa}j})}.$$

The error calculation assumed $\delta\omega = 1\,\%$, $\delta n = 10\,\%$, $\delta I = 5\,\%$, $\delta\lambda = 10\,\%$.

Depth profiling results are listed in Tables 3 and 4.

Total niobium nitride film thickness in both cases is approximately the same: (5.0 ± 0.4) nm for the $NbN/SiO_2/Si$ film, and (4.3 ± 0.4) nm for the NbN/Sp film. An interface layer is formed when niobium nitride is deposited onto the SiO_2/Si substrate, this is not observed when niobium nitride is deposited on the sapphire substrate. Air oxidation of both films results in formation of the same oxide layers and a layer with a different niobium nitride phase.

Table 3. Chemical depth profiling of the oxidized ultrathin film $NbN/SiO_2/Si$

Layer	d, nm	Chemical formula
6	1.56 ± 0.23	$0.60Nb_2O_5 + 0.40Nb_2O_{5x}$
5	0.72 ± 0.13	$0.56NbNO_x + 0.40NbO_2$
4	2.18 ± 0.29	NbN_x
3	2.8 ± 0.3	NbN
2	1.02 ± 0.18	$NbN\text{-}SiO_2$
1	3.4 ± 0.4	SiO_2
Substrate	∞	Si

Table 4. Chemical depth profiling of the oxidized ultrathin NbN/Sp film

Layer	d, nm	Chemical formula
4	1.53 ± 0.23	$0.73Nb_2O_5 + 0.27Nb_2O_{5x}$
3	0.59 ± 0.11	$0.43NbNO_x + 0.57NbO_2$
2	2.9 ± 0.3	NbN_x
1	1.43 ± 0.20	NbN
Substrate	∞	Al_2O_3

2.2. Air-oxidized ultrathin niobium nitride films on the silicon substrate before and after relaxation

Ultrathin niobium nitride film was formed in the same way as the films described in the previous section. Substrate — SiO_2/Si (oxidized silicon). Sputtered film thickness is 2–3 nm.

After fabrication and removal from the sputtering chamber, the ultrathin film was subjected to air oxidation during 10 h. Then, the film was placed into the analytical chamber. The first spectrum was recorded two days after the film fabrication; this spectrum is hereinafter referred to as the spectrum before relaxation. After this, the film was removed from the vacuum chamber and film relaxation in vacuum took place. The second spectrum measured after three weeks is hereinafter referred to as the spectrum after relaxation.

Elemental analysis of the ultrathin niobium nitride film identified the following elements: Nb, C, O, N, Si.

Phase analysis of the ultrathin NbN film on the SiO_2/Si substrate was performed simultaneously with the N $1s$, O $1s$, Nb $3d$, Si $2p$ spectral photoelectron lines. When a sample contains complex (two-/three-component) compounds, they shall be detected on all spectral photoelectron lines of the elements included in these compounds.

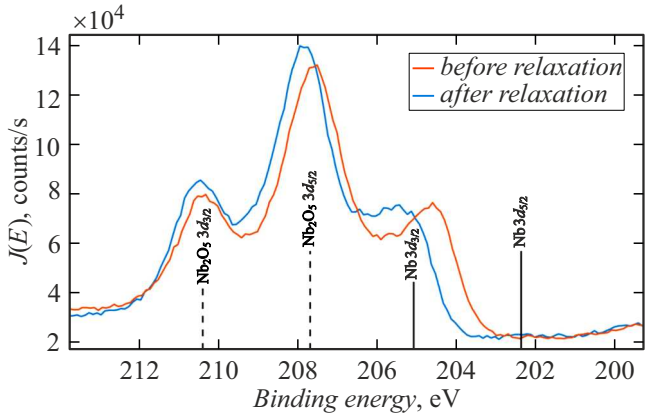

Figure 4. Nb 3*d* X-ray photoelectron spectral line from the ultrathin NbN/SiO_2/Si film before and after relaxation.

Figure 4 shows the experimental Nb 3*d* lines. A spectrum recorded before relaxation is shown with a blue solid line, a spectrum recorded after relaxation is shown with a red solid line. It can be seen that the niobium nitride phase is modified during relaxation.

Analysis of photoelectron lines in the film spectrum identified the following: Nb 3*d* line before and after film relaxation — the same phases of NbN and NbN_x and Nb_2O_5, Nb_2O_{5x}, $NbNO_x$; N 1*s* line before film relaxation — NbN, NbN_x, $NbNO_x$; O 1*s* lines before film relaxation — Nb_2O_5, Nb_2O_{5x}, NbO_x phases, SiO_2 and CO_x; Si 2*p* line before film relaxation — SiO_2 and Si. Analysis of all these spectral lines also identified the NbN-SiO_2 interface phase. The identified phases and their binding energies in ultrathin films before and after relaxation are shown in Table 5.

For depth profiling, a target model is introduced. It is known from the film fabrication history that niobium was deposited in nitrogen and argon atmosphere onto an oxidized silicon substrate. Then, atmospheric oxidation occurred, and the higher oxide, Nb_2O_5, film was formed on top. The phase analysis detected niobium suboxide and $NbNO_x$ phases. These phases will be assigned to the same layer between the top oxides layer and niobium nitride. The identified various niobium nitride phases are located in different layers. A phase related to the NbN-SiO_2 interface layer between the substrate and niobium nitride film was also identified.

Layer thicknesses were calculated using equation (1). Depth profiling results before and after relaxation are listed in Tables 6 and 7.

Total thickness of the ultrathin niobium nitride film (excluding layers 1 and 6) is the same before and after relaxation: (3.7 ± 0.3) nm silicon oxide layer and SiO_x-NbN_x interface layer thicknesses remain unchanged during relaxation. Phase composition of the film is modified during relaxation: the highest oxide and $NbNO_x$ layers get thinner and the NbN_x layer gets thicker.

2.3. Air-oxidized ultrathin NbN/GaN films with and without a protective resistive layer

The process of forming niobium nitride films on gallium nitride is described in [17]. The gallium nitride buffer layer was grown on a sapphire base by the chemical vapour deposition method. Niobium nitride films were formed using the Orion magnetron sputtering system made by AJA International Inc. Some films were coated with a resistive layer after deposition, which should significantly decelerate niobium nitride film oxidation. The resulting films were controlled by the HRTEM method. The image (Figure 5) taken from [17] shows that niobium nitride and gallium nitride have a single-crystal structure and their

Table 5. Phase depth profiling of the ultrathin NbN/SiO_2/Si film

Chemical formula	Binding energy, eV							
	Before relaxation				After relaxation			
	Nb 3*d*	N 1*s*	O 1*s*	Si 2*p*	Nb 3*d*	N 1*s*	O 1*s*	Si 2*p*
NbN	205.3	397.2	–	–	205.1	397.0	–	–
NbN_x	204.7	398.2	–	–	204.4	398.3	–	–
$NbNO_x$	205.8	399.6	531.4	–	205.7	399.6	–	–
NbN-SiO_2	206.7	401.0	532.4	102.5	206.4	401.0	–	102.1
Nb_2O_5	207.6	–	530.7	–	207.5	–	–	–
Nb_2O_{5x}	208.1	–	530.7	–	208.0	–	–	–
Si	–	–	–	100.1	–	–	–	99.8
SiO_2	–	–	533.1	103.7	–	–	–	103.4
CO_x	–	–	533.8	–	–	–	–	–

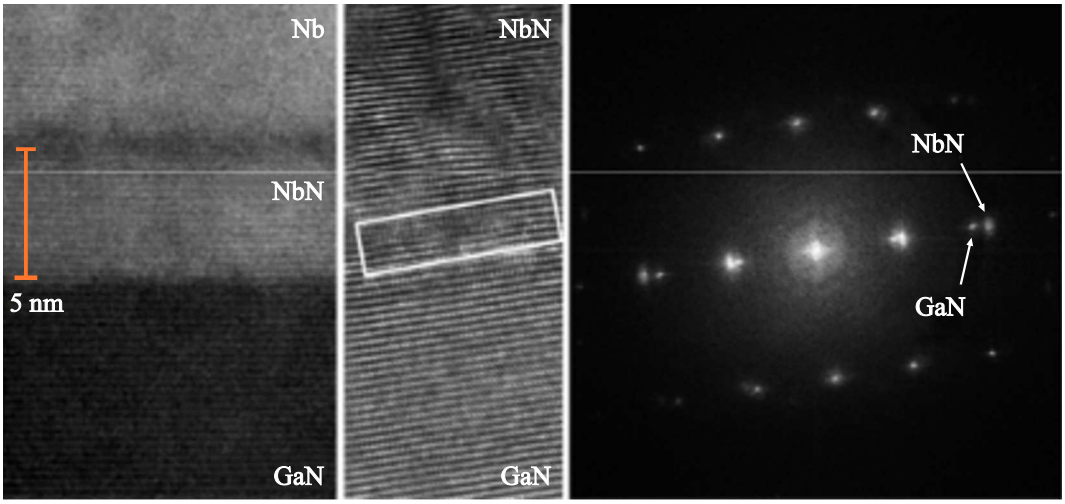

Figure 5. HRTEM cross-sectional image of the NbN/GaN film.

Table 6. Chemical depth profiling of the oxidized ultrathin $NbN/SiO_2/Si$ film before relaxation

Layer	d, nm	Chemical formula
6	2.12 ± 0.28	$0.64Nb_2O_5 + 0.36Nb_2O_{5x}$
5	0.92 ± 0.16	$NbNO_x$
4	0.62 ± 0.11	NbN_x
3	1.14 ± 0.19	NbN
2	0.99 ± 0.17	SiO_x-NbN_x
1	3.2 ± 0.4	SiO_2
Substrate	∞	Si

Table 7. Chemical depth profiling of the oxidized ultrathin $NbN/SiO_2/Si$ film after relaxation

Layer	d, nm	Chemical formula
6	2.01 ± 0.27	$0.61Nb_2O_5 + 0.39Nb_2O_{5x}$
5	0.44 ± 0.08	$NbNO_x$
4	1.17 ± 0.19	NbN_x
3	1.07 ± 0.18	NbN
2	0.99 ± 0.17	SiO_x-NbN_x
1	3.2 ± 0.4	SiO_2
Substrate	∞	Si

lattices coincide almost perfectly. The niobium nitride layer thickness is approximately 5 nm.

Before spectral measurement, the protective resistive layer was fully removed from the films, for which the film was held in acetone during 15 min. Before loading into the chamber, the films were held in isopropyl alcohol for about 10 min. The films were not subjected to ion beam evaporation in the chamber.

Examination of the samples several weeks after their preparation [17] showed that the oxide layer thickness of the samples coated with a resistive layer was less than 1 nm, and of the samples without a resistive layer was about 2 nm (see also [23]). The examination was repeated after 5 months, the results are given in this work; oxide layer thicknesses in both cases are much the same and equal to about 2 nm. Therefore, a conclusion is made that the resistive layer decelerates the film oxidation process, rather than prevents it. As will be shown below, the difference of the chemical composition of films is in that a different niobium nitride phase is formed under the oxide layer, when the film has been previously coated with a resistive layer, compared with the natural film oxidation.

In Section 2.3, the ultrathin film with a protective resistive layer, that has been removed before spectrum recording, is denoted as „Film 1“, and the film without a previously applied protective resistive layer is denoted as „Film 2“.

Elemental analysis of ultrathin (NbN/GaN/Sp) films 1 and 2 identified the following elements: Nb, O, N, C, Ga, Na. Aluminum was not detected. Thus, the thickness of the layers above the sapphire substrate is greater than the probing depth. Figure 6 shows survey X-ray photoelectron spectra of films 1 and 2, Figure 7 shows the Nb 3d line spectra: blue solid line — film 1, red solid line — film 2.

Phase depth profiling of ultrathin films 1 and 2 was performed simultaneously on the Nb 3d and N 1s spectral photoelectron lines. It can be seen that the phase composition of ultrathin films with and without a previously applied protective resistive layer is different. Analysis of the photoelectron lines in the spectra of ultrathin films 1 and 2 detected the following: N 1s and Nb 3d lines — various NbN and NbN_x phases; Nb 3d line — Nb_2O_5, Nb_2O_{5x},

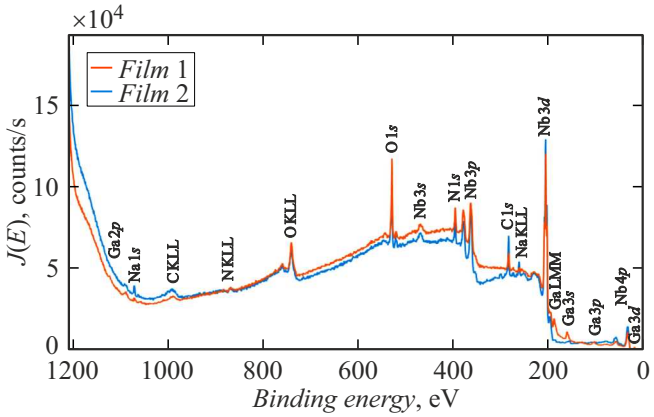

Figure 6. Survey X-ray photoelectron spectra of ultrathin NbN/GaN/Sp films with a previously applied protective resistive layer (film 1) and without such layer (film 2).

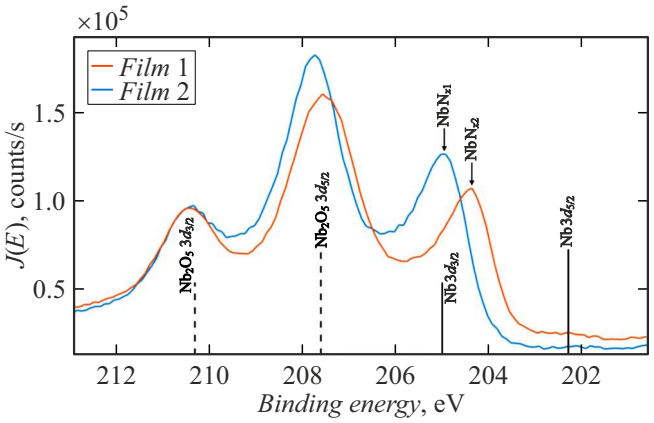

Figure 7. X-ray photoelectron spectrum of the Nb 3*d* line of ultrathin films 1 and 2.

Table 8. Phase depth profiling of ultrathin films 1 and 2

Chemical formula	Binding energy, eV			
	Film 1		Film 2	
	Nb 3*d*	N 1*s*	Nb 3*d*	N 1*s*
NbN	205.3	397.2	205.3	396.8
NbN_x	204.8	398.5	204.3	397.8
$NbNO_x$	206.3	–	206.3	–
Nb_2O_5	207.6	–	207.6	–
Nb_2O_{5x}	208.6	–	208.6	–

$NbNO_x$. The detected phases and their binding energies are shown in Table 8. Layer thicknesses were calculated using equation (1). Depth profiling results are listed in Tables 9 and 10.

Table 9. Chemical depth profiling of ultrathin film 1

Layer	*d*, nm	Chemical formula
5	1.87 ± 0.26	$0.85Nb_2O_5 + 0.15Nb_2O_{5x}$
4	1.00 ± 0.17	$NbNO_x$
3	3.5 ± 0.4	NbN_{x1}
2	3.21 ± 0.29	NbN
1	Undefined	GaN

Table 10. Chemical depth profiling of ultrathin film 2

Layer	*d*, nm	Chemical formula
5	1.82 ± 0.26	$0.89Nb_2O_5 + 0.11Nb_2O_{5x}$
4	0.98 ± 0.17	$NbNO_x$
3	3.4 ± 0.4	NbN_{x2}
2	1.56 ± 0.21	NbN
1	Undefined	GaN

The presence of the protective resistive layer (film 1) leads to a slower film oxidation resulting in formation of a different niobium nitride phase than that of film 2 without the protective resistive layer, during air oxidation. Stoichiometric coefficient x_1 is approximately equal to 1, stoichiometric coefficient x_2 is about 0.75.

2.4. Air-oxidized ultrathin NbN/GaN films after sputtering and oxidation

Film 1 (see Section 2.3) was subjected to argon ion beam sputtering during 20 min, after evaporation a photoelectron spectrum was recorded. This film is hereinafter referred to as „Film 3“. Then film 3 was moved from the analytical chamber into a lock chamber where it was held in air for 10 min. This film is hereinafter referred to as „Film 4“. Then, film 4 was returned from the lock chamber into the analytical one and a photoelectron spectrum was recorded.

Elemental analysis of ultrathin (NbN/GaN/Sp) films 3 and 4 identified the following elements: Nb, O, N, C, Ga. Elemental analysis of the ultrathin film changed during the air oxidation period due to carbon deposition (there was no carbon after argon ion beam evaporation).

Phase analysis of ultrathin films 3 and 4 was performed simultaneously on the Nb 3*d*, N 1*s*, O 1*s* and C 1*s* spectral photoelectron lines. Analysis of the photoelectron lines in the spectra of ultrathin films 3 and 1 detected the following: Nb 3*d* and N 1*s* lines — various NbN and NbN_x phases; Nb 3*d* line — Nb_2O_5, Nb_2O_{5x}, NbO_2. $NbNO_x$ phase was detected in the Nb 3*d* line spectrum of film 4. The detected phases and their binding energies are shown in Table 11. Figure 8 shows X-ray photoelectron spectra of

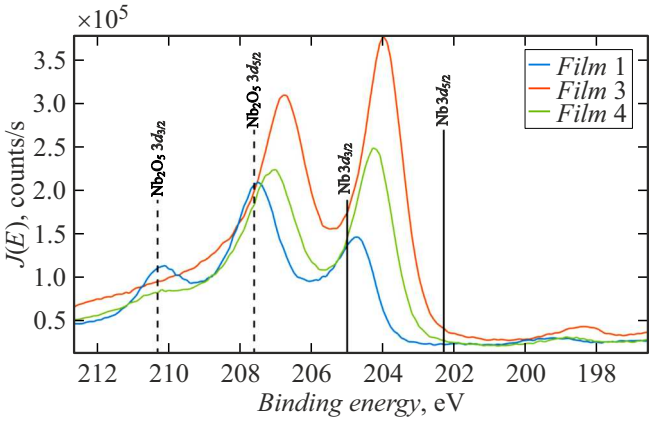

Figure 8. X-ray photoelectron spectrum of the Nb 3d line of ultrathin films 1, 3 and 4.

Table 11. Phase analysis of ultrathin films 3 and 4

Chemical formula	Binding energy, eV			
	Film 3		Film 4	
	Nb 3*d*	N 1*s*	Nb 3*d*	N 1*s*
NbN	205.3	397.2	205.3	396.8
NbN_x	204.0	397.8	204.2	397.9
$NbNO_x$	–	–	205.5	400.0
Nb_2O_5	207.6	–	207.6	–
Nb_2O_{5x}	208.7	–	208.7	–
NbO_2	206.5	–	206.5	–

the Nb 3*d* lines from ultrathin films 1, 3 and 4. Blue solid line shows the spectra of film 1, red solid line shows the spectra of film 3, green solid line shows the spectra of film 4. Layer thicknesses were calculated using equation (1). Depth profiling results are listed in Tables 12 and 13.

During argon ion sputtering of film 1, oxide layer was removed and niobium nitride phase was modified (NbN_x binding energy on the Nb 3*d* line for film 1 was 204.8 eV, and after sputtering (for film 3) was 204.0 eV). During oxidation, the niobium nitride phase also changes: NbN_x binding energy on the Nb 3*d* line for film 4 was equal to 204.2 eV.

Conclusion

The study investigated various ultrathin niobium nitride films that differed in the type of substrate, surface oxidation time and rate, and ion beam impact. Ultrathin niobium nitride films were formed using the Orion magnetron sputtering system (AJA International Inc.). For each of the films, film formation and photoelectron spectra measurement processes are described, elemental analysis, quantitative analysis with relative concentration measurement, phase analysis, depth profiling with thickness measurement, chemical and phase composition of layers were carried out. The effect of film history on the chemical phase layer-by-layer profile is investigated.

The following ultrathin films for cryogenic nanoelectronics were analyzed.

• Ultrathin niobium nitride films on silicon oxide-on-silicon (SiO_2/Si) and sapphire (Sp) substrates deposited by the magnetron sputtering method. The films were subjected to atmospheric oxidation during several days. Total niobium nitride film thickness in both cases is approximately the same: (5.0 ± 0.4) nm for the NbN/SiO_2/Si film, and (4.3 ± 0.4) nm for the NbN/Sp film. An interface layer is formed when niobium nitride is deposited onto the SiO_2/Si substrate, this is not observed when niobium nitride is deposited on the sapphire substrate. Air oxidation of both films results in formation of the same oxide layers.

• Ultrathin niobium nitride film on the silicon substrate before and after relaxation. After fabrication and removal from the sputtering chamber, the film was subjected to atmospheric oxidation. The first spectrum was recorded during two days after the film formation, after that the film was not removed from the vacuum chamber and film relaxation took place in vacuum during three weeks. Total thickness of the ultrathin niobium nitride film is the same before and after relaxation: (3.7 ± 0.3) nm. silicon oxide layer and SiO_x-NbN_x interface layer thicknesses remain unchanged during relaxation. Phase composition of the film is modified during relaxation: the higher oxide and $NbNO_x$ layers get thinner and the NbN_x layer gets thicker.

• Ultrathin niobium nitride films on gallium nitride (NbN/GaN/Sp). Some films were coated with a resistive

Table 12. Chemical depth profiling of ultrathin film 3

Layer	*d*, nm	Chemical formula
4	0.68 ± 0.12	$0.44Nb_2O_5 + 0.20Nb_2O_{5x} + 0.36NbO_2$
3	3.1 ± 0.3	NbN_x
2	1.26 ± 0.20	NbN
1	Undefined	GaN

Table 13. Chemical depth profiling of ultrathin film 4

Layer	d, nm	Chemical formula
4	1.02 ± 0.17	$0.52Nb_2O_5 + 0.16Nb_2O_{5x} + 0.25NbO_2 + 0.07NbNO_x$
3	3.1 ± 0.3	NbN_x
2	1.50 ± 0.23	NbN
1	Undefined	GaN

layer. Oxide layer thickness and phase composition depend on the niobium nitride film oxidation time and rate. The effect of argon ion beam sputtering and air oxidation was investigated. Ion impact and air oxidation leads to formation of a layer with a niobium nitride phase other than the original one.

Funding

The study was funded by the Ministry of Science and Higher Education of the Russian Federation under state assignment № FSWF-2023-0016.

Conflict of interest

The authors declare no conflict of interest.

References

[1] E.M. Gershenzon, G.N. Gol'tsman, I.G. Gogidze, Y.P. Gusev, A.I. Elant'ev, B.S. Karasik, A.D. Semenov. Sov. Phys. Superconductivity, **3**, 1582 (1990).
[2] G.N. Gol'tsmanD.I. Ludkov. Izvestiya vuzov. Radiofizika, **46** (8–9), 671 (2003) (in Russian).
[3] G.N. Gol'tsman, O. Okunev, G. Chulkova, A. Lipatov, A. Semenov, K. Smirnov, B. Voronov, A. Dzardanov, C. Williams, R. Sobolewski. Appl. Phys. Lett., **79** (6), 505 (2001). DOI: 10.1063/1.1388868
[4] M.I. Finkel, Yu.B. Bakhtomin, S.V. Antipov, S.N. Maslennikov, N.S. Kaurova, G.N. Goltsman. *Teragertsovye smesiteli na effekte elektronnogo razoreva v ultratonkikh plenkakh NbN i NbTiN* (MPGU, M., 2015) (in Russian)
[5] O.V. Minaeva, O.V. Okunev, G.M. Tchulkova. *Bystrodeistvuyushchii odonofotonnyi detektor na osnove tonkoi sverkhprovodnikovoi plenki NbN* (Prometei, M., 2013) (in Russian)
[6] P. Zolotov, A. Divochiy, Y. Vakhtomin, V. Seleznev, P. Morozov, K. Smirnov. KnE Energy, **3** (3), 83 (2018). DOI: 10.18502/ken.v3i3.2016
[7] N.A. Saveskul, N.A. Titova, E.M. Baeva, A.M. Semenov, A.V. Lubenchenko, S. Saha, H. Reddy, S.I. Bogdanov, E.E. Marinero, V.M. Shalaev, A. Boltasseva, V.S. Khrapai, A.I. Kardakova, G.N. Goltsman. Phys. Rev. Appl., **12** (5), 054001 (2019). DOI: 10.1103/PhysRevApplied.12.054001
[8] M. Kroug, S. Cherednichenko, H. Merkel, E. Kollberg, B. Voronov, G. Gol'tsman, H.-W. Hübers, H. Richter. IEEE Transactions on Appl. Superconductivity, **11** (1), 962 (2001). DOI: 10.1109/77.919508
[9] T. Shiino, S. Shiba, N. Sakai, T. Yamakura, L. Jiang, Y. Uzawa, H. Maezawa, S. Yamamoto. Superconductor Sci. Technol., **23** (4), 045004 (2010). DOI: 10.1088/0953-2048/23/4/045004
[10] J.R. Gao, M. Hajenius, F.D. Tichelaar, T.M. Klapvijk, B. Voronov, E. Grishin, G. Gol'tsman, C.A. Zorman, M. Mehregany. Appl. Phys. Lett., **91** (6), 062504 (2007). DOI: 10.1063/1.2766963
[11] S. Krause, D. Meledin, V. Desmaris, A. Pavolotsky, V. Belitsky, M. Rudziński, E. Pippel. Superconductor Sci. Technol., **27** (6), 065009 (2014). DOI: 10.1088/0953-2048/27/6/065009
[12] A. Darlinski, J. Halbritter. Surf. Interface Analysis, **10** (5), 223 (1987). DOI: 10.1002/sia.740100502
[13] A.V. Lubenchenko, A.A. Batrakov, A.B. Pavolotsky, S. Krause, I.V. Shurkaeva, O.I. Lubenchenko, D.A. Ivanov. EPJ Web of Conferences, **132**, 03053 (2017). DOI: 10.1134/S1027451018040134
[14] A. Ermolieff, M. Girard, C. Raoul, C. Bertrand, T.M. Duc. Appl. Surf. Sci., **21** (1), 65 (1985). DOI: 10.1016/0378-5963(85)90008-X
[15] B.A. Gurovich, K.E. Prihod'ko, M.A. Tarkhov, E.A. Kuleshova, D.A. Komarov, V.L. Stolyarov, E.D. Ol'shanskii, B.V. Goncharov, D.A. Goncharova, L.V. Kutuzov, A.G. Domantovskii, Z.V. Lavrukhina, M.M. Dement'eva. Nanotechnol. Russia, **10** (7), 530 (2015). DOI: 10.1134/S1995078015040072
[16] G. Oya, Y. Onodera. J. Appl. Phys., **45** (3), 1389 (1974). DOI: 10.1063/1.1663418
[17] S. Krause, V. Afanas'ev, V. Desmaris, D. Meledin, A. Pavolotsky, V. Belitsky, A. Lubenchenko, A. Batrakov, M. Rudzińsky, E. Pippel. IEEE Transactions Appl. Super-conductivity, **26** (3), 1 (2016). DOI: 10.1109/TASC.2016.2529432
[18] S. Krause, V. Mityashkin, S. Antipov, G. Gol'tsman, D. Meledin, V. Desmaris, V. Belitsky, M. Rudzińsky. IEEE Transactions on Terahertz Sci. Technol., **7** (1), 53 (2017). DOI: 10.1109/TTHZ.2016.2630845
[19] A. Semenov, B. Günther, U. Böttiger, H.-W. Hübers, H. Bartolf, A. Engel, A. Schilling, K. Ilin, M. Siegel, R. Schneider, D. Gerthsen, N.A. Gippius. Phys. Rev. B, **80** (5), 054510 (2009). DOI: 10.1103/PhysRevB.80.054510
[20] A.V. Lubenchenko, O.I. Lubenchenko, D.A. Ivanov, D.S. Lukuantsev, A.B. PavolotskyO.N. Pavlov, I.V. Ivanova. ZhTF, **94** (8), 1229 (2024) (in Russian). DOI: 10.61011/JTF.2024.08.58550.112-24
[21] A.V. Lubenchenko, A.A. Batrakov, I.V. Shurkaeva, A.B. Pavolotsky, S. Krause, D.A. Ivanov, O.I. Lubenchenko. J. Surf. Investigation, **12** (4), 692 (2018). DOI: 10.1134/S1027451018040134

[22] A.V. Lubenchenko, A.A. Batrakov, A.B. Pavolotsky, O.I. Lubenchenko, D.A. Ivanov. Appl. Surf. Sci., **427**, 711 (2018). DOI: 10.1016/j.apsusc.2017.07.256
[23] A.V. Lubenchenko, A.A. Batrakov, S. Krause, A.B. Pavolotsky, I.V. Shurkaeva, D.A. Ivanov, O.I. Lubenchenko. J. Phys.: Conf. Ser., **917**, 092001 (2017). DOI: 10.1088/1742-6596/917/9/092001

Translated by E.Ilinskaya